



## Impact of spatio-temporal heterogeneities and lateral stirring and mixing on mid-water biotic interactions

E. Martinez<sup>\*</sup>, K.J. Richards

International Pacific Research Center, School of Ocean and Earth Science and Technology, University of Hawaii at Manoa, Honolulu, Hawaii, USA

### ARTICLE INFO

#### Article history:

Received 11 December 2009  
Received in revised form 1 April 2010  
Accepted 14 April 2010  
Available online 24 April 2010

#### Keywords:

Particle flux  
Modeling  
Mesopelagic zone  
Ecosystems  
Mesoscale processes

### ABSTRACT

We study the impact of spatial and temporal inhomogeneities in the flux of particles on particle–biology interactions in the mesopelagic zone using a flux–prey–predator model. The mid-water biology is found to affect significantly the carbon flux associated with the sinking particles. Although the annual mean export flux at the bottom of the zone (taken to be at 1000 m depth) is changed at most 25% in the experiments reported here, the timing and amplitude of pulses of the bottom flux are very dependent on the way the flux at the top of the zone (taken to be 100 m depth) is packaged in time and space. The apparent sinking speed, based on the arrival of pulses of the export flux at the bottom of the zone (1000 m), can vary from 5 m day<sup>−1</sup> to 30 m day<sup>−1</sup>. Lateral stirring and mixing also impact the temporal and spatial distributions of the particle flux. A useful metric in determining the impact of stirring and mixing is the “mix-down depth” which combines the effects of the initial patch size, strength of stirring, diffusion and sinking rate. When the mix-down depth is small compared to the depth to which biological interactions are important, then the impact of stirring and mixing is large, producing significant changes to the temporal behavior of the export flux and reducing spatial inhomogeneities. The results have implications for the sampling of the carbon flux associated with sinking particles and the representativeness of point measurements.

© 2010 Elsevier B.V. All rights reserved.

### 1. Introduction

Over the last decade, the JGOFS community has undertaken an extensive series of marine biogeochemical field studies (Doney et al., 2002). One of the aims is to determine the processes that control partitioning of carbon and related biological components within the ocean and at the ocean–atmosphere boundary (Doney et al., 2002). With regard to climate change, the carbon cycle has been the focus of a number of efforts (Andersson et al., 2004; Baker, 2007; Tortell et al., 2008). Most of the studies and models concentrate on the euphotic zone. The sampling in the mesopelagic zone is difficult, and as such the biochemical processing of mid-water marine particles is not well known. This issue, however, is gaining increasing attention (Dadou et al., 1996; Jackson and Burd, 2002; Stemann et al., 2004a,b). In the mesopelagic zone, the vertical flux of carbon associated with sinking particles, hereafter referred to as the “particle flux”, has the largest decrease; the particles undergo a transformation by biological (grazing and bacterial degradation) and physical mechanisms (stirring and mixing). Only about 10% of the flux which leaves the bottom of the euphotic zone (typically about 100 m) reaches 1000 m (Martin et al., 1987; Stemann et al., 2004b), representing a significant reduction in

the carbon exported to the deep ocean; 45% of the open ocean particulate organic carbon (POC) flux at 1000 m reaches the sea floor where it is partly oxidized or sequestered in sediments (Jahnke, 1996). Thus, the transfer of carbon through the mid-water marine reservoir plays a key role in controlling the sequestration of atmospheric CO<sub>2</sub>.

The decrease in particle flux in biochemical mesopelagic models is often represented as a function of depth only with either a power law or an exponential dependence (Martin et al., 1987; Armstrong et al., 2002). However, biochemical transformations need to be included (Stemann et al., 2004b). Dadou et al. (1996) developed a 1-D model that predicts the vertical flux of elements in mid-water and deep-water as a function of surface inputs. They suggested that adding marine snow dynamics or zooplankton behavior could improve their results. For the latter, Jackson and Burd (2002) developed a 1-D flux–prey–predator model to describe the impacts of the animal interactions on the particle vertical flux. They also considered bacterial degradation through the bacterial remineralization and consumption of the sinking particulate organic carbon. The consideration of animals in their model of carbon flux and remineralization provides an added dimension for controlling particle flux, as organism dynamics can affect remineralization rates. Recent works (Dadou et al., 1996; Jackson and Burd, 2002; Laws, 2004; Stemann et al., 2004a,b) emphasize the understanding of biogeochemical processes as crucial in any attempts to estimate what controls the vertical flux of materials.

Both the spatial and temporal variability in the flux at the top of the mesopelagic zone reflect the physical forcing and the responses of

<sup>\*</sup> Corresponding author. Present location: UPMC University of Paris 06, UMR 7093, Laboratoire d’Océanographie de Villefranche (LOV), CNRS, 06230 Villefranche-sur-Mer, France.

E-mail address: [martinez@obs-vlfr.fr](mailto:martinez@obs-vlfr.fr) (E. Martinez).

the biological community in the upper layers of the ocean. Surface heterogeneities can be induced by locally forced phenomenon such as fronts and mesoscale eddies (Dadou et al., 1996) and induced upwelling and/or phytoplankton blooms, occurring over short or seasonal (at high latitudes) period. This variability will propagate through the water column. Many global models have explicitly modeled the euphotic zone. However, to date, no study has specifically investigated carbon export with a dedicated 3-D biochemical model in the mid-water column, despite the fact the flux is known to be patchy in both space and time (Stemmann et al., 2008). Here we investigate how the distribution of the surface flux affects the particle flux and the dynamics of the biological system within the mesopelagic zone. We utilize the model of Jackson and Burd (2002) for the particle/biological interactions within the water column. The model is forced by the flux of particles at the top (surface) of the mesopelagic zone. Because of nonlinearities in the biological component, the same total flux distributed differently in time and/or space will not necessarily result in the same processing of particles and the same eventual carbon export.

Interactions within the biological system are also affected by the presence of the eddying motions of the fluid flow. In the euphotic zone the stirring and mixing by eddies are known to impact the ecosystem dynamics (see e.g. Richards and Brentnall, 2006). It is unclear how important eddy stirring and mixing are on the dynamics of the mesopelagic system. Here we evaluate the impact.

The rest of the paper is organized as follows. In Section 2 we describe the bio-physical model used in the study. In Section 3 the results are presented of a series of numerical experiments designed to elucidate the impact of heterogeneity in the mesopelagic system. The paper closes with a discussion in Section 4.

## 2. Method

The spatio-temporal evolution of the mesopelagic ecosystem is determined by an advection–reaction–diffusion equation; advection because the system is under the influence of the fluid flow, reaction because species  $C(\mathbf{X}, t)$  interact and diffusion because turbulence or molecular random motions mix properties. For the case of an incompressible velocity field  $\mathbf{V}(\mathbf{X}, t)$ , the standard form of these equations is:

$$\frac{\partial C(\mathbf{X}, t)}{\partial t} = R(C, \mathbf{X}) + D\nabla^2 C(\mathbf{X}, t) - \mathbf{V}(\mathbf{X}, t) \cdot \nabla C(\mathbf{X}, t) \quad (1)$$

where  $C = [C_1, C_2, C_3, \dots]$  represents the state vector of species,  $D$  is the diffusivity tensor (set to be the same for all components) and  $R$  the reaction terms.

### 2.1. The mesopelagic flux–prey–predator model

The region of interest is the mesopelagic zone, typically taken to be the 100–1000 m depth range, which is below the euphotic zone, and where no further photosynthetic production takes place.

The ecosystem model employed here is that of Jackson and Burd (2002). Three trophic levels are considered: the flux of falling particles ( $F$ ) and two levels of the zooplankton community with the particle feeding animals ( $P$ ) and the predatory animals ( $Q$ ) concentrations. With no horizontal variations or fluid flow the system is governed by the following equations:

$$\begin{aligned} \frac{\partial F}{\partial t} &= -v \frac{\partial F}{\partial z} - \sigma v P F - \lambda F \\ \frac{\partial P}{\partial t} &= +a\sigma P F - b P Q \\ \frac{\partial Q}{\partial t} &= +c b P Q - d Q. \end{aligned} \quad (2)$$

Variability in  $F$  is brought about by a loss/gain caused by the sinking of particles with a velocity  $v$ , the loss of particles grazed by the particle feeders where  $\sigma$  is the interaction coefficient for flux feeding, and the bacterial degradation of particles at a rate  $\lambda$ . Variability of  $P$  at a given depth results from growth by particle feeding ( $a$  is the conversion efficiency of  $F$  to  $P$ ), a loss due to predation ( $b$  is the interaction coefficient). The time evolution of  $Q$  results from the difference in the feeding on  $P$  ( $c$  is an efficiency factor) and death, with  $d$  the specific mortality rate of predators. The steady-state concentrations at a given depth ( $F_s, P_s$  and  $Q_s$ ) for a spatial homogeneous case are (Jackson and Burd, 2002):

$$\begin{aligned} F_s &= F_0 e^{-kz} \\ P_s &= \frac{d}{bc} \\ Q_s &= \frac{a\sigma F_0}{b} e^{-kz} \end{aligned} \quad (3)$$

where  $F_0$  is the flux at the top of the mesopelagic zone and  $k = \sigma P_s + \lambda/v$  is the vertical decrease constant. The exponential component in Eq. (3) indicates an exponential decrease with depth of both  $F$  and  $Q$ . The parameters used in Eqs. (1), (2) and (3) are presented in Table 1. Their corresponding values are defined according to the study of Jackson and Burd (2002).

Jackson and Burd (2002) show the 3 parameters that control the behavior of the system. These are: the relative size of flux fluctuations ( $\gamma$ ), the effect of animal vertical movement ( $K_z$ ), the functional form of mortality (here taken to be linear:  $dQ$ ) and the bacterial degradation rate ( $\lambda$ ). With no external changes in particle flux ( $\gamma = 0$ ),  $P$  and  $Q$  populations display the classical Lotka–Volterra oscillation. Because changes in the particle flux leaving the surface cause large (chaotic) oscillations in the zooplankton communities, experiments with different surface forcing imply different  $F$ – $P$ – $Q$  interactions and hence the timing and shape of the flux to the benthos. Considering the Jackson and Burd (2002) sensitivity tests on  $\gamma$  we choose an intermediate value of 0.5. They also tested the animal vertical movement parameter modeled by vertical diffusion. Consistent with their study, the vertical motion is considered to be random for both particle

**Table 1**  
Parameters and values summary following Jackson and Burd (2002).

Parameter	Description	Value	Units
$a$	Conversion factor from particle to particle feeder	0.3	Dimensionless
$b$	Rate coefficient for predation on particle feeder	123	$\text{m}^3 \text{gC}^{-1} \text{day}^{-1}$
$c$	Conversion factor from particle feeder to predator	0.3	Dimensionless
$d$	Specific mortality rate of predator	0.01	$\text{day}^{-1}$
$F_0$	Flux leaving the surface	0.1	$\text{gC m}^{-2} \text{day}^{-1}$
$\lambda$	Specific rate of bacterial degradation	$6.25 \times 10^{-4}$ (low activity) 0.1285 (high activity)	$\text{day}^{-1}$
$\sigma$	Particle feeding coefficient	15	$\text{m}^2 \text{gC}^{-1}$
$v$	Vertical velocity	30	$\text{m day}^{-1}$
$\omega$	Frequency of perturbations in flux	$2\pi/365$	$\text{day}^{-1}$
$K_z$	Vertical diffusion parameter	$10^{-3}$	$\text{m}^2 \text{s}^{-1}$
$\gamma$	Relative size of the temporal fluctuations in the flux	0.5	Dimensionless

feeders and carnivores and is modeled with the same vertical diffusion parameter  $K_z$  in the following equations:

$$\begin{aligned}\frac{\partial F}{\partial t} &= -v\frac{\partial F}{\partial z} - \sigma vPF - \lambda F \\ \frac{\partial P}{\partial t} &= +a\sigma PF - bPQ + K_z\frac{\partial^2 P}{\partial z^2} \\ \frac{\partial Q}{\partial t} &= +cbPQ - dQ + K_z\frac{\partial^2 Q}{\partial z^2}.\end{aligned}\quad (4)$$

An increase of  $K_z$  decreases the range of  $P$  and increases the spatial coherence. We consider the animal populations to have random vertical movements, with an implied vertical diffusivity  $K_z$  (which very crudely models the vertical migration of animals). The inclusion of vertical diffusion synchronizes the Lotka–Volterra oscillations in the  $P$  and  $Q$  populations, which would otherwise act independently at each depth level. However, a too large value of  $K_z$  dampens these oscillations. We take  $K_z = 10^{-3} \text{ m}^2 \text{ s}^{-1}$ , an intermediate value in the 3 experiments performed by Jackson and Burd (2002). The predator quadratic mortality in the Jackson and Burd (2002) model tends to dampen fluctuations in the bottom flux. The observations of Smith and Kaufmann (1999), which show that the variability in the bottom flux is relative to that at the surface, supports our choice of a linear mortality formulation. We also considered a low and high value of bacterial activity. In a bacterially dominated particle degradation case, the  $F$ – $P$ – $Q$  concentrations at 1000 m are strongly decreased and may prevent us to elucidate the impact of the surface flux variability and of the stirring and mixing. To be illustrative, the average export flux at 1000 m is 0.4% (25%) of the prescribed flux at 100 m under high (low) bacterial activity for Run 1D-2 (see Section 3.1.1). Most of the results we present here are for the case of relatively low bacterial activity.

## 2.2. Lateral advection and diffusion model

The ecosystem exists in a fluid ocean. To quantify the impact of the fluid flow we consider a simple two-dimensional kinematic flow field that produces chaotic mixing. The stirring in the horizontal of the biogeochemical tracers produces thin filaments of tracer (by stretching and folding) that are eventually mixed through the imposed diffusion. The flow field was introduced by Pierrehumbert (1994) and used by Richards and Brentnall (2006) to study the impact of stirring and mixing on the euphotic zone ecosystem. The velocity components  $U(x, y, t)$  and  $V(x, y, t)$  in the two horizontal dimensions  $x$  and  $y$ , respectively, are given by:

$$\begin{aligned}U(x, y, t) &= \frac{A}{T}\theta\left(\frac{T}{2} - t(\text{mod}T)\right)\sin\left(\frac{2\pi y}{L} + \phi_i\right) \\ V(x, y, t) &= \frac{A}{T}\theta\left(t(\text{mod}T) - \frac{T}{2}\right)\sin\left(\frac{2\pi x}{L} + \phi_{i+1}\right).\end{aligned}\quad (5)$$

The sinusoidal shear flow alternates along the  $x$  and  $y$  directions for each half-period ( $T/2$ ) and is constant with depth. The amplitude parameter  $A$  sets the stirring intensity.  $\theta$  is the Heaviside step function and  $\phi_i$  is a randomly distributed phase between  $[0, 2\pi]$  set at each half-period, to avoid transport barriers in the flow.  $L$  is the width of the domain. Decreasing  $T$  increases the stirring rate of the flow. The stirring characteristics of the flow are further described in Section 3.2.

Diffusion is taken into account and directly implemented in the numerical model using  $K_m$ , the horizontal diffusion coefficient. It is related to  $D$  in Eq. (1). The parameters used in Eqs. (5), (6), (7) and (8) are presented in Table 2.

**Table 2**

Summary of the physical model parameters.

Parameter	Description	Value	Units
$A$	Stirring intensity	$0.7 \times L$	m
$T$	Period of the sinusoidal shear flow	4	day <sup>-1</sup>
$\phi_i$	Randomly distributed phase	$[0, 2\pi]$	rad
$L$	Width of the domain	6000	m
$n$	Control of the time-width of the bloom	1 (simple sinusoid) 32 (sharp peak)	Dimensionless
$\gamma_2$	Relative size of the spatial fluctuations in the flux	0.5	Dimensionless
$k_L$	Horizontal wave number	$2\pi/L$	m <sup>-1</sup>
$m$	Control of the space-width of the bloom	1 (simple sinusoid) 32 (sharp peak)	Dimensionless
$v$	Vertical propagation speed of the signal	30	m day <sup>-1</sup>
$\mu$	Lyapunov exponent	$1.66/T$	day <sup>-1</sup>
$L_p$	Horizontal scale of a patch	$L/4$ (Run 3D-2)	m
$K_m$	Horizontal diffusion coefficient	0.1	m <sup>2</sup> s <sup>-1</sup>
$w_f$	Width of filaments	$\sqrt{K_m/\mu}$	m
TMZ	Top of the mesopelagic zone	100	m
BMZ	Bottom of the mesopelagic zone	1000	m

## 2.3. Numerical details

The calculations are performed between the top of the mesopelagic zone (TMZ: here taken to be at 100 m depth, see Table 2), and the bottom of the mesopelagic zone (BMZ: here taken to be at 1000 m depth). The model is forced by specifying the particle flux,  $F_{zo}(x, y, t)$  at the TMZ (see Section 2.4), the flux being modified by biological processes as the particles sink through the water column. The water column is discretized into 101 layers (a vertical grid spacing of 9 m).

Advection of biological tracers is carried out using an upstream finite difference scheme (Smolarkiewicz, 1983; Smolarkiewicz and Margolin, 1998), with explicit diffusion (Smolarkiewicz and Clarck, 1986) to represent subgrid-scale advective processes. Divergent flow and monotonicity options (Smolarkiewicz and Grabowski, 1990; Smolarkiewicz and Margolin, 1998) are used. The Multidimensional Positive Definite Advection Transport Algorithm (MPDATA) scheme is implemented for biological tracers to ensure that the transport is positively definite.

Both physical and ecological models are solved on a  $32 \times 32$  doubly periodic grid within a square domain of width  $L$ . This is only a moderate horizontal resolution, chosen by consideration of the required computer resources, but it will not affect unduly the conclusions drawn on the effects of stirring and mixing. The width  $L$  is chosen in relation to the size of the lateral diffusion coefficient so that the lateral structure of the tracer fields is resolved (see Section 3.2).

The initial conditions are taken to be the steady state (neglecting animal movement) (Eq. (3)) and the system integrated forward in time with a timestep of 0.01 day (8645 s). The results presented for the 1 dimensional model in Section 3 have been integrated over 6 years. Considering the exported flux at the BMZ, it follows an approximately regular annual cycle by the second year. The results for the 3 dimensional model are presented therefore for the second year of integration, again for computer resource considerations. The near periodic nature of the results for the particle flux at the BMZ suggests that the 3 dimensional model is also close to a regular annual cycle by this time (Non-periodic behavior of  $P$  and  $Q$  in the deeper layers in year 2 was found for some experiments, but because of the very low values of both  $P$  and  $Q$  at these depths this is not expected to affect the results significantly.).

## 2.4. The surface flux at the top of mesopelagic zone (TMZ)

A feature of production in the euphotic zone is its patchiness in both space and time (Martin, 2003) which will be reflected in patchiness in

the particle flux to depth. To investigate the impact of this patchiness, the particle flux at the TMZ,  $F_{zo}$ , is the combination of temporal ( $f_{ot}$ ) and spatial ( $f_{os}$ ) components.

$$\begin{aligned} f_{ot}(t) &= \gamma \cdot (\sin(\omega t) + 1)^n \\ f_{os}(x, y) &= \gamma_2 \cdot (\sin(k_L \cdot x) \sin(k_L \cdot y) + 1)^m \\ F_{zo}(x, y, t) &= F_0(f_{ot} \cdot A_t + \varepsilon_t)(f_{os} \cdot A_s + \varepsilon_s) \end{aligned} \quad (6)$$

The frequency of the perturbed flux  $\omega$  is set to be  $\omega = 2\pi/\text{year}$ . The minimum (background) and maximum values with respect to time are given by  $\varepsilon_t$  and  $A_t$ , respectively. We choose  $\varepsilon_t$  and  $A_t$  such that the temporal integral of the first bracketed term is 1. The time-width of the “bloom” is controlled by  $n$  which is an integer (the higher the value of  $n$  the sharper the peak in the flux). We consider two bloom temporal widths with  $n = 1$  (a simple sinusoid) and  $n = 32$  (a sharp peak localized in time). For reference, Jackson and Burd (2002) consider a flux of the form  $F_{zo}(t) = F_0(1 + \gamma \sin(\omega t))$ , which is equivalent to setting  $A_t = 1$ ,  $\varepsilon_t = 1 - \gamma$  (with  $\gamma = 0.5$ ) and  $n = 1$ . In all cases the phase of the temporal signal is chosen such that the maximum occurs at day 91 in the results presented below.

The spatial variability in the horizontal ( $x, y$ ) space is controlled in a similar manner, where the horizontal wave number,  $k_L$ , is chosen to be equal to zero for the horizontally homogeneous case (labeled as 1D) and equal to  $2\pi/L$  for the 3D configurations (i.e. wave number 1 in both directions over the domain, labeled as 3D), and  $\gamma_2 = 0.5$ . The spatial-width of the “bloom” is controlled by  $m$  (an integer). As with time, we set the spatial-width by choosing  $m = 1$  and 32, and  $\varepsilon_s$  and  $A_s$  such that the spatial integral of the first bracketed term is 1. The various combinations of  $n$ ,  $m$  and  $k_L$  used in the numerical experiments are given in Table 3.

### 3. Results

In presenting the results we separate out the impact of the form of the flux at the TMZ into the impact of the temporal variability of the flux (1D-1 and 1D-2 in Table 3) and the impact of spatial variability of the flux for a given temporal variability (3D-1 and 3D2). The impact of stirring and mixing is considered last.

#### 3.1. Impact of the temporal and spatial heterogeneity of the flux at the TMZ

##### 3.1.1. Sinusoidal and short pulse bloom events

The results from the flux–prey–predator 1-D model (i.e.  $k_L = 0$ ) with low bacteria activity, forced with an annual sinusoidal flux at the TMZ,  $F_{zo}$  ( $n = 1$ ), is shown in Fig. 1 upper row (Run 1D-1 in Table 1) (Note, the forcing has the same form as that used by Jackson and Burd, 2002). As the particle flux ( $F$ ) increases at the TMZ so do the near-surface particle feeders ( $P$ ) reducing significantly the flux of particles to depth. After a short lag time the carnivores ( $Q$ ) start to graze  $P$ . Grazing by  $Q$  severely restricts the growth of  $P$  such that the maximum concentration at the TMZ ( $2 \text{ mg C m}^{-3}$ ) occurs before the maximum in the forcing flux (by 51 days) and such that the subsequent near-surface particle flux is little affected by consumption by  $P$ . The carnivores reach a maximum value ( $1.8 \text{ mg C m}^{-3}$ ) a little while (27 days) after the maximum in  $P$ . The cycle is completed by the

death of  $Q$  caused by the lack of  $P$  which occurs on a relatively slow timescale determined by the mortality rate  $d$ . At depth we see a “shadow” zone in  $F$  underneath the high production period whose trailing edge propagates downwards at the particle sinking rate. This is followed by a propagating wave of  $F$ ,  $P$  and  $Q$  whose speed, at approximately  $5 \text{ m day}^{-1}$ , is much slower than the particle sinking speed ( $30 \text{ m day}^{-1}$ ). The crash in  $P$  at the surface means that the sinking particles are little affected. As these particles sink below the region of high  $Q$ , however, the particle feeders are able to utilize the food source, with again a delayed response in  $Q$ .

Setting the forcing flux at the TMZ to have a high amplitude pulse over a short time period ( $n = 32$ , Run 1D-2), the simulation reflects a spring bloom (Fig. 1 lower row). The ratio  $F_{\max}/F_{\min}$  of the flux at the TMZ is almost 4 times higher than in Run 1D-1. The greater and faster surface flux in Run 1D-2 prompts a more rapid and stronger growth in  $P$ , and an associated larger reduction in  $F$  which provides a near-surface double maximum. As before we see a propagating wave-like disturbance, although now because of the more rapid decrease in  $F$  at the TMZ with time the depth penetration is less than with  $n = 1$ , and the propagation speed (defined as the slope of a maxima or minima) is somewhat faster, at approximately  $11.5 \text{ m day}^{-1}$ . After a depth of around 400 m the impact of  $P$  on  $F$  is reduced and the sinking speed of the signal in  $F$  eventually reaches the sinking speed of the particles.

The timing and amplitude of the pulses in export flux (the particle flux at the BMZ) are very much a function of the flux at the TMZ and the mid-water biological interactions. Fig. 2 shows the export flux as a function of time for Runs 1D-1 and 1D-2. For Run 1D-1, we see a number of small local maxima with the main pulse arriving at the end of the year, i.e. 275 days after the maximum in  $F$  at the TMZ. For Run 1D-2 the net result of the particle feeders on the particle flux is that the particles arrive in two pulses centered on Days 96 and 138, respectively. Averaged over the year the export flux for Run 1D-1 is  $0.033 \text{ g C m}^{-2} \text{ day}^{-1}$ , i.e.  $0.33F_0$  (see Table 1). The larger biological response in Run 1D-2 produces a reduced average export flux of  $0.25F_0$ . For reference, with no biology (i.e.,  $P = Q = 0$ ) except bacterial degradation the maximum in export flux would occur 30 days after the maximum in the flux at the TMZ, i.e. on Day 121 (figure not shown), and the average export flux would be  $0.57F_0$ .

As we will see in the experiments described below the production of multiple pulses of particle flux together with on occasion the slowing down of the propagation of these pulses are common features of the system. Unfortunately, because of the non-linearity of the system, we have not been able to derive an analytical expression for the speed of descent in terms of the particle flux and biological parameters.

An alternative view of Runs 1D-1 and 1D-2 is shown in Fig. 3a and b, respectively, where  $P$  is plotted against  $Q$  as a function of depth. As well as the larger response in  $P$  and  $Q$  in Run 1D-2 ( $(P_{\max}, Q_{\max}) = (13.2 \text{ mg C m}^{-3}, 6.8 \text{ mg C m}^{-3})$ ) versus  $(2.3 \text{ mg C m}^{-3}, 1.9 \text{ mg C m}^{-3})$  in Run 1D-1, there is also a more rapid reduction in their values with depth. They reach 50% of their maximum values at the TMZ after 4.2 days (126 m below the surface) and 5.5 days (165 m) for run 1D-1 and after only 1.5 days (45 m) and 2.5 days (75 m) for run 1D-2, respectively.

For comparison the case of Run 1D-2 with the higher bacteria activity ( $\lambda$ ) is shown in Figs. 2c and 3c. The bacterial consumption of  $F$  becomes stronger with a consequent reduction in the response of  $P$  and  $Q$  which is confined closer to the surface (Fig. 3c with  $(P_{\max}, Q_{\max}) = (10.1 \text{ mg C m}^{-3}, 4.6 \text{ mg C m}^{-3})$ ). The export flux averaged over the year is now reduced to  $0.004 F_0$ , with the reduction dominated by bacterial degradation. Biological (animals + bacterial) activity does affect, however, the temporal distribution of the export flux. Again we see two peaks but with the first peak significantly larger than the second and arriving at Day 108 (Fig. 2c), i.e. 12 days before the peak expected with low bacterial activity. To emphasize the impact of spatial variability, advection and diffusion on the particle flux and the biological communities the remaining results are

**Table 3**  
Spatial and temporal characteristics used in the numerical experiments.

Name	Dimensions	$n$	$m$	$k_L$	1 year average export flux at the bottom
1D-1	1-D	1	0	0	$0.33 F_0$
1D-2	1-D	32	0	0	$0.25 F_0$
3D-1	3-D	1	1	$2\pi/L$	$0.33 F_0$
3D-2	3-D	32	32	$2\pi/L$	$0.26 F_0$

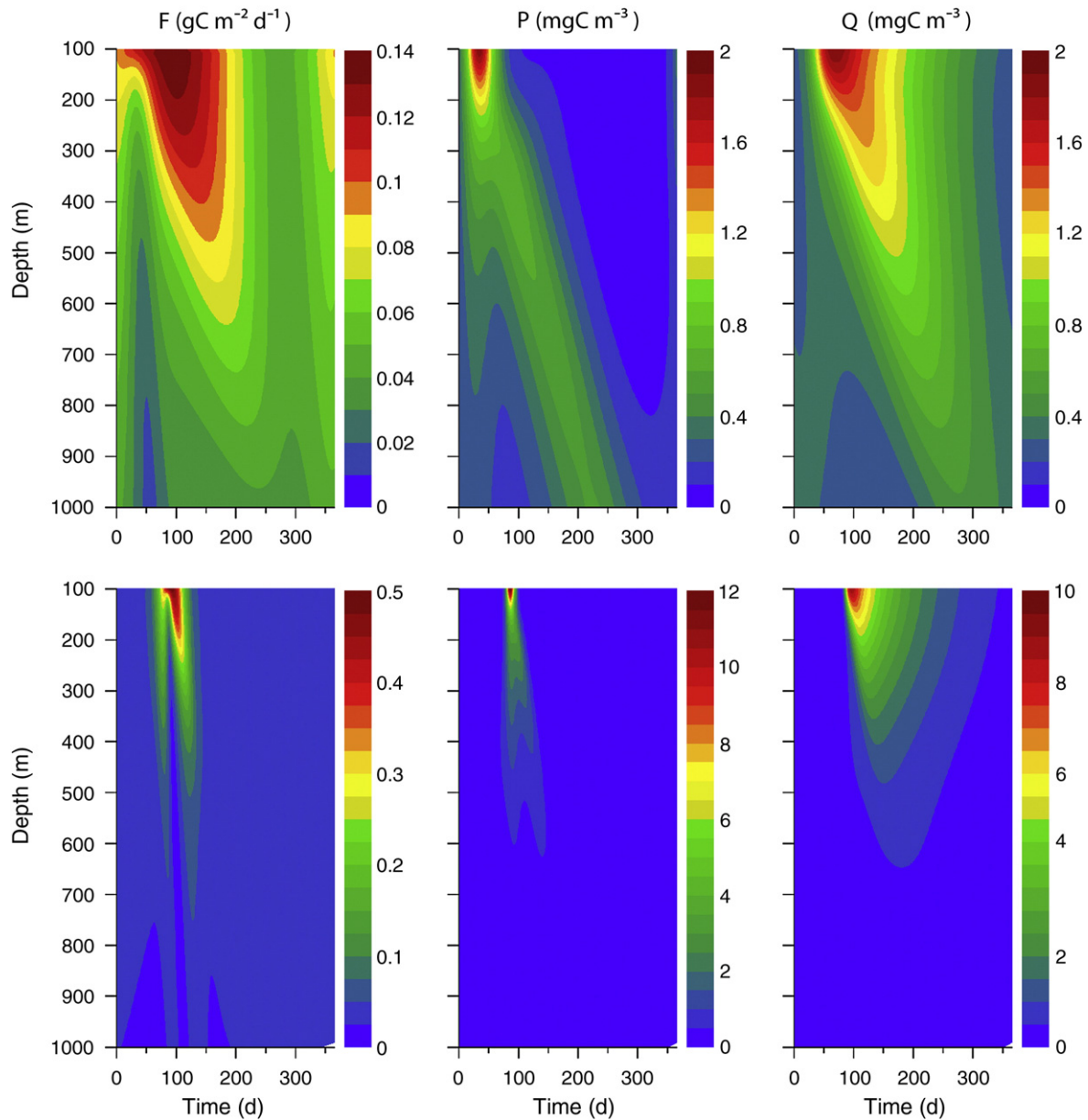


Fig. 1. Time evolution against depth of  $F$  (left panels),  $P$  (center panels) and  $Q$  (right panels) in the 1-D model with low bacteria activity and  $n = 1$  (upper row),  $n = 32$  (bottom row).

presented from experiments with the lower bacterial activity, although it is recognized that the results are dependent on the poorly known role of microbial activity.

### 3.1.2. Spatial patchiness (with no advection or diffusion)

The 3-D model allows us to investigate the role played by patchiness in the flux at the TMZ on predator–prey interactions. With no advection or diffusion, changes to the overall behavior of the model are brought about solely by the way the flux at the TMZ is distributed into regions of high and low flux. The two time-forcing cases presented in the previous section ( $n = 1$  and 32) are considered in regard to a sinusoidal spatial distribution ( $m = 1$ , Run 3D-1) and a strong localized patch in the flux at the TMZ ( $m = 32$ , Run 3D-2) (see Table 3).

Fig. 4 shows the time series of  $F$ ,  $P$  and  $Q$  at the top of the domain at the locations of maximum and minimum flux ( $F_{\text{high}}$  and  $F_{\text{low}}$ , respectively) for Runs 3D-1 and 3D-2. The time evolution of  $P$  and  $Q$  varies considerably at the two locations for both runs and reflects

the magnitude of the overwintering carnivore population. With the choice of forcing (Eq. (6)) the minimum flux at the TMZ is greater at  $F_{\text{high}}$  than  $F_{\text{low}}$ . Consequently the carnivore concentration  $Q$ , before the bloom, is at a higher level at  $F_{\text{high}}$  compared to  $F_{\text{low}}$  and therefore able to respond faster to the increased  $P$  concentration. At  $F_{\text{low}}$  the delayed  $Q$  response allows the growth in  $P$  to last longer such that  $P$  reaches its maximum at a later time. The effect is particularly marked in Run 3D-2 where, despite the lower flux at  $F_{\text{low}}$ ,  $P$  reaches a higher maximum value than at  $F_{\text{high}}$ .

The export flux, under the high and low flux regions at the TMZ for Runs 3D-1 and 3D-2, are shown in Fig. 5. Averaged over the year the export flux compared to their respective values at the TMZ for the high (low) flux regions are  $0.34F_{\text{high}}$  ( $0.32F_{\text{low}}$ ) for Run 3D-1 and  $0.25F_{\text{high}}$  ( $0.26F_{\text{low}}$ ) for Run 3D-2. The timing and relative intensity of pulses in export flux are different under the high and low flux regions. For 3D-2 the differences are such that the maximum export flux arrives at approximately Day 220 under the high flux region, while it arrives at Day 100 under the low flux region. Averaged over the horizontal

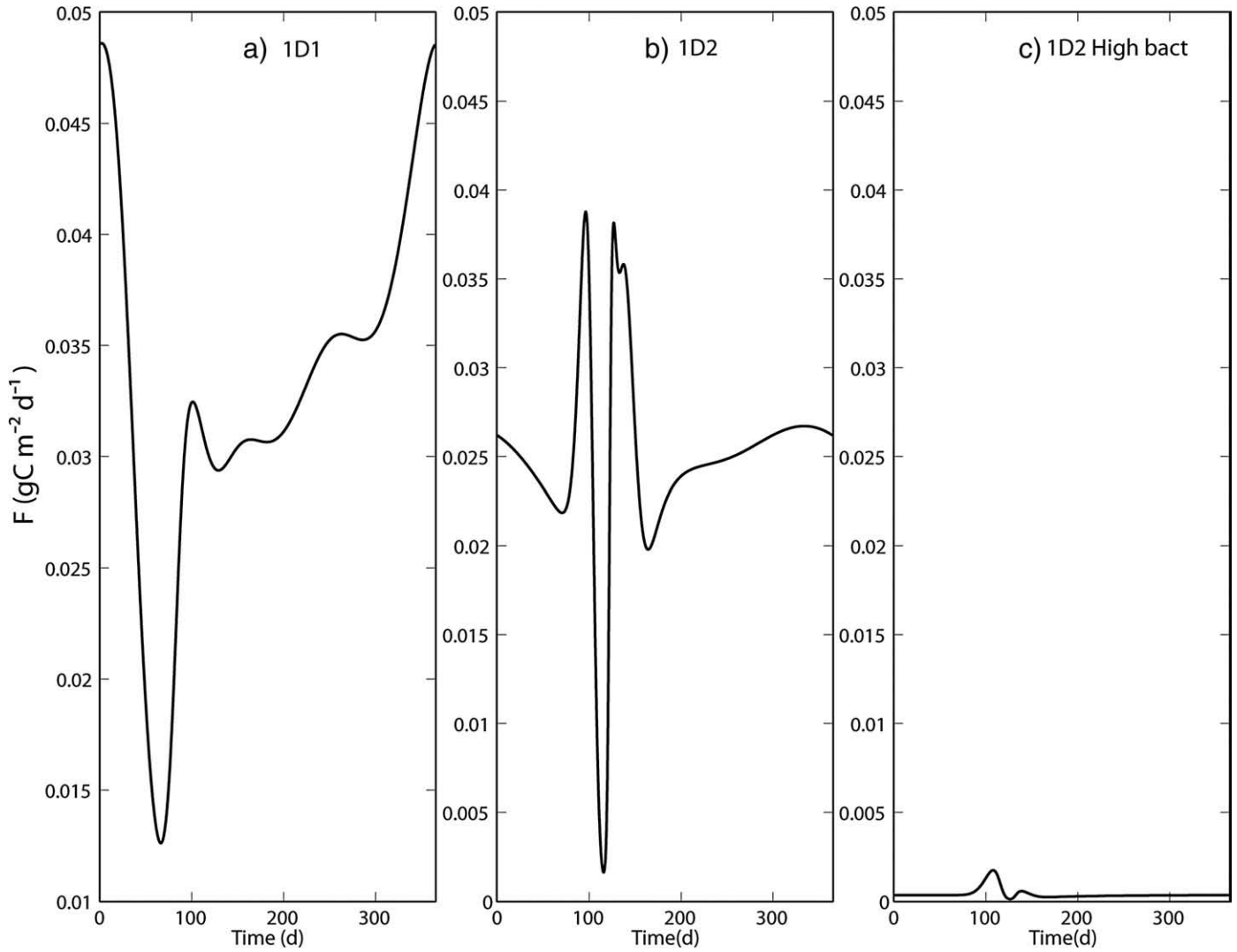


Fig. 2. Export flux for a)  $n = 1$  (1D-1), b)  $n = 32$  (1D-2) both with a low bacteria activity ( $\lambda = 6.25 \times 10^{-4} \text{ day}^{-1}$ ), and c) 1D-2 with high bacteria activity ( $\lambda = 0.1285 \text{ day}^{-1}$ ).

domain and over the year, the export flux is  $0.33 F_0$  and  $0.26 F_0$  for Runs 3D-1 and 3D-2, respectively; values that are surprisingly close to the equivalent 1D experiments given the very different responses of  $P$  and  $Q$  at the TMZ and the different temporal distributions of the export flux

under the high and low flux regions (see Table 3). For Run 3D-1, as with Run 1D-1 the spatially averaged maximum export flux occurs at the end of the year (Fig. 5). For 3D-2 the second maximum at Day 150 is suppressed while there is broader maximum centered on Day 230.

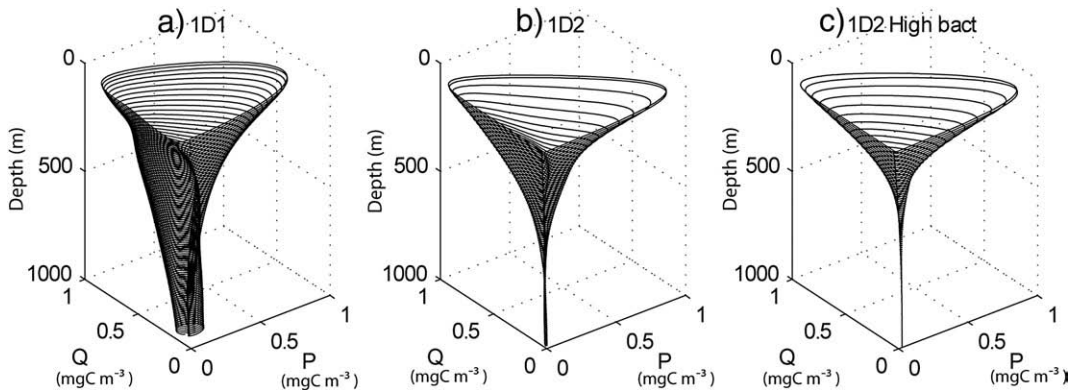


Fig. 3. Three-dimensional phase plots. Variation in the concentration of  $P$  and  $Q$  as a function of depth (in meters) for the 3 cases shown in Fig. 2.  $P$  and  $Q$  concentrations are normalized by their maximum values respectively.

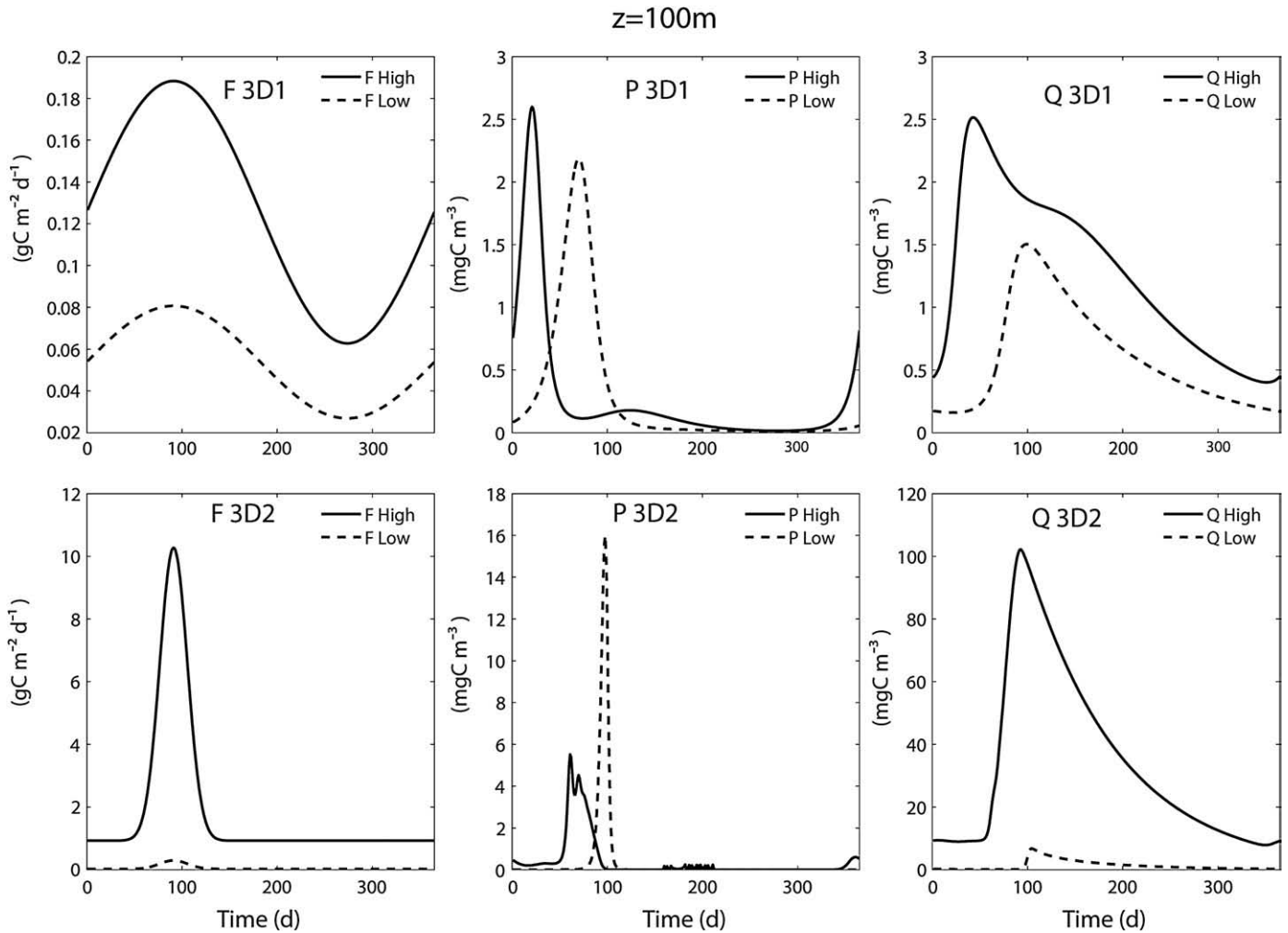


Fig. 4. Time series at the top of the MPZ ( $z = 100$  m) for the Runs 3D-1 (top panels) and 3D-2 (bottom panels).  $F$  (left),  $P$  (center) and  $Q$  (right) at the same location as the high (solid line) and low (dashed line) surface fluxes.

### 3.2. Impact of stirring and mixing

Horizontal stirring is an additional mechanism that induces strong inhomogeneities and which is inherent in the open ocean. Here we consider advection by a chaotic flow given by (Eq. (5)), which is uniform with depth. The ratio  $A/L$  controls the geometric properties of the stirring and  $T$  the speed of stirring without altering the trajectories of the fluid element (Neufeld et al., 2002). We set  $A/L = 0.7$ , in which case the flow is nearly ergodic (Neufeld et al., 2002). In a chaotic flow, fluid elements separate exponentially at a rate given by the Lyapunov exponent,  $\mu$ , which can be taken as a measure of the stirring rate of the flow. For the flow defined in Eq. (5)  $\mu \approx 1.66/T$ , and is uniform across the domain.

The addition of mixing will tend to reduce the inhomogeneities of biogeochemical properties induced by the forcing at 100 m and the fluid stirring (as well as affect the reaction rates between species; Eq. (1)). As the particles fall to depth the horizontal distribution of the particles and associated biogeochemical properties will tend to become more homogenous through the action of the fluid stirring and mixing. An important measure of the mixing, therefore, is the depth at which properties become essentially horizontally homogenized. We refer to this depth as the *mixing*, or *mix-down depth*,  $L_d$  (Eqs. (7)–(8), see Table 2). We may expect the impact of stirring and mixing to depend on how  $L_d$  compares with the depth over which significant biological reactions take place,  $L_b$ . If  $L_d \gg L_b$ , then the stirring and mixing will have little effect. As  $L_d/L_b$  tends to zero the system should behave as the

horizontally homogeneous case. For a steady forcing  $L_b$  is given by  $1/k$  from Eq. (3). For the biological parameters chosen (c.f. Table 1) this gives  $L_b \sim 250$  m. This value gives a reasonable estimate for the unsteady forcing cases also, based on the rate of decrease with depth of  $P$  and  $Q$  found in the numerical experiments.

We can convert the *mix-down depth* to a *mix-down time*  $T_m$ , by  $T_m = L_d/v$ , where  $v$  is the vertical propagation speed of the signal. Pulses of  $F$  have different propagation speeds, as in the 1D case (and looking forward to Fig. 7). Averaged over the depth of the domain the propagation speeds of the two pulses are approximately equal to  $30 \text{ m day}^{-1}$  (the particle sinking rate) and  $18 \text{ m day}^{-1}$ , respectively. At a given depth, we therefore expect the second pulse to arrive in a more homogeneous state than the first because of the longer time the fluid stirring and mixing has had to act. Our estimate of  $T_m$  depends on the ratio  $L_p/w_f$ , where  $L_p$  is the horizontal scale of a patch (in our case the width of the region of high surface flux), and  $w_f$  is the width of filaments created by the stirring and diffusion (where  $w_f = \sqrt{K_m/\mu}$  and  $K_m$  is the horizontal diffusion coefficient), which expresses a balance between the thinning of tracer filaments by the straining of the flow and a broadening by diffusion. For  $L_p/w_f \gg 1$  the *mix-down time* is appropriate, i.e. the time it takes for the stirring to stir down the initial patch to the width of the filaments (Thuburn and Tan, 1997; Hu and Pierrehumbert, 2001a,b), by which time the tracer will be spread across the domain and subsequent folding by the flow will produce rapid mixing. The mix-down time is found by Richards and Brentnall (2006) to be a key parameter in the impact of stirring and

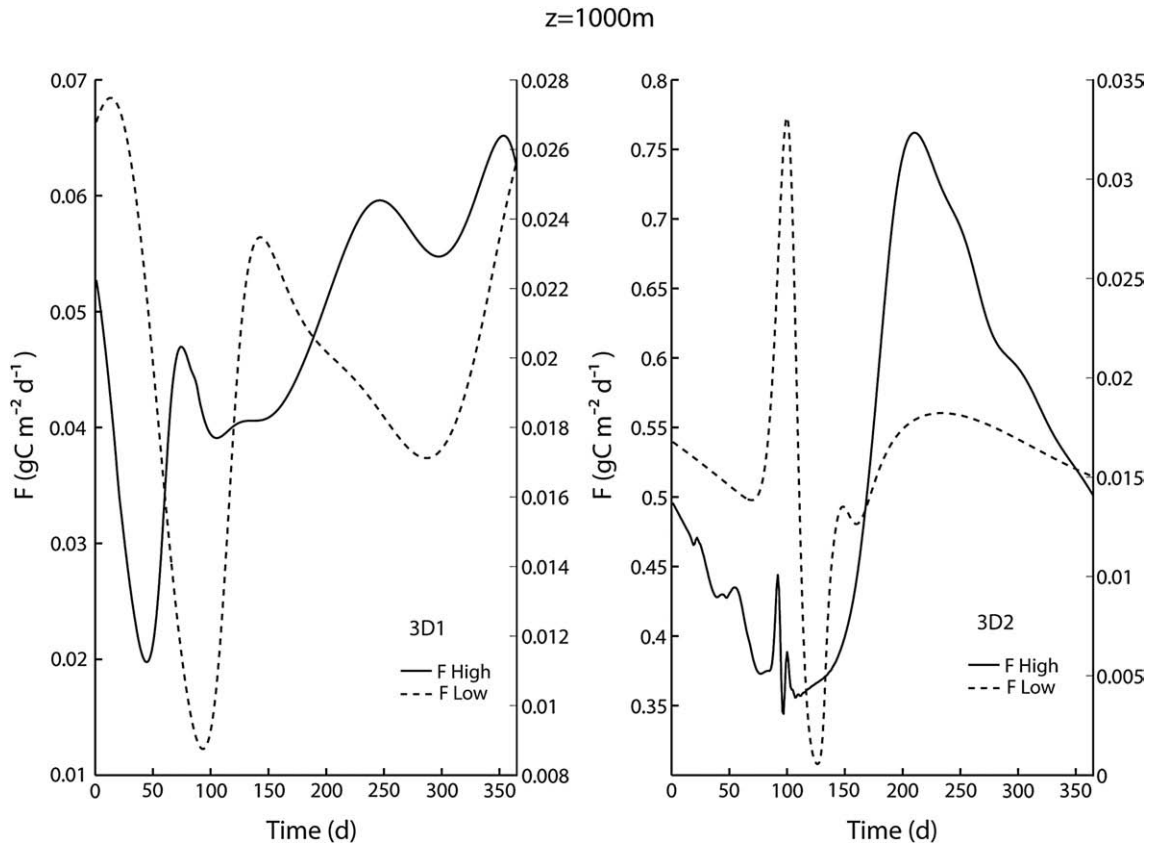


**Fig. 5.** Export flux ( $F$  at  $z = 1000$  m) for Run 3D-1 (left panel) and Run 3D-2 (right panel) at the location of the high (solid line, left axes) and low (dashed line, right axes) surface fluxes.

mixing on the marine ecosystems in the euphotic zone. In this case the mix-down depth is given by:

$$L_d = \frac{v}{\mu} \ln \left( \frac{L_p}{w_f} \right). \quad (7)$$

If  $L_p/w_f \approx 1$  or less then we need to look at the time it takes for the tracer to be spread across the domain which will be related to the Lagrangian integral timescale of the flow (Garrett, 1983). The mix-down depth is now expected to be given by:

$$L_d = \frac{v}{\mu} \left( 2 \frac{L_p}{w_f} - 1.5 - 0.5 \frac{L_p^2}{w_f^2} \right). \quad (8)$$

For the parameters chosen, Eq. (7) applies to all the cases considered here.

To illustrate the impact of stirring and mixing we can vary the mix-down depth by varying respectively  $T$  or  $K_m$ . Here we present results from experiments 3D-2, where the forcing flux at the TMZ  $F_{zo}$  is localized in both time ( $n = 32$ ) and space ( $m = 32$ ). The mix-down depth for the cases considered below is given in Table 4 using  $v = 30 \text{ m day}^{-1}$  (appropriate for the first pulse in  $F$ ). The mix-down depth for the second pulse is approximately half this value.

**Table 4**

Mix-down depth  $L_d$  (meters) for different  $T$  (days) and  $K_m$ , and for different surface forcing. Note depths are relative to the top of the mesopelagic zone (TMZ).

Run 3D-2 ( $n$ and $m = 32$ )	$K_m = 0.1 \text{ m}^2 \text{ s}^{-1}$	$K_m = 1 \text{ m}^2 \text{ s}^{-1}$
$T = 26$ days	682	141
$T = 4$ days	173	90

For the lateral diffusion coefficient, representing small scale processes, we set  $K_m = 0.1 \text{ m}^2 \text{ s}^{-1}$  (which is similar to the value found by Ledwell et al., 1998, for the initial dispersion of a tracer released in the thermocline and which is consistent with the estimate of Young et al., 1982, based on the combined effects of internal gravity waves and vertical diffusion). We also consider the effects of increasing the diffusion coefficient to  $K_m = 1.0 \text{ m}^2 \text{ s}^{-1}$ . We consider  $T = 4$  days and  $T = 26$  days. With these choices of  $K_m$  and  $T$ ,  $L_d$  varies by a factor of 7.5.

For  $K_m = 0.1 \text{ m}^2 \text{ s}^{-1}$  the filament width  $w_f$  (the e-folding width) is approximately 0.2 km. We choose the domain width  $L$ , therefore, to be 6 km so that the filaments are resolved. This is a small size domain. Our results can be applied directly to larger size domains by scaling the value of  $K_m$  with  $L^2$ . Note that the amplitude of the advection is already scaled with  $L$ .

Before considering the vertical variation of the system we consider the horizontal distribution of the particle flux,  $F$ , at the bottom of the mesopelagic zone (BMZ). Fig. 6 shows  $F$  at the BMZ for the unstirred and the 4 stirred cases considered, at Day 90 (the approximate time when the first pulse of particles arrives). The stirring and mixing by the flow have spread the signal across the domain with greater stirring (smaller  $T$ ) and greater diffusion (larger  $K_m$ ) producing a more uniform distribution (note the color scales vary on the individual plots). Although the mix-down depth given by Eq. (7) and Table 4 is only a crude measure, it is consistent with the results shown in Fig. 6 with respect to the implied tendencies induced by changes in the stirring or mixing.

Fig. 7 compares the spatially averaged depth/time evolution of  $F$ ,  $P$  and  $Q$  for case 3D-2 for 3 different stirring and mixing regimes (unstirred,  $T = 26$  days and 4 days with  $K_m = 0.1 \text{ m}^2 \text{ s}^{-1}$ ). Fig. 8 shows  $P$  plotted against  $Q$  as a function of depth.  $P_{\max}$  and  $Q_{\max}$  values are  $(14.1; 6.8) \text{ mg C m}^{-3}$  for the unstirred case. Close to the TMZ the effect

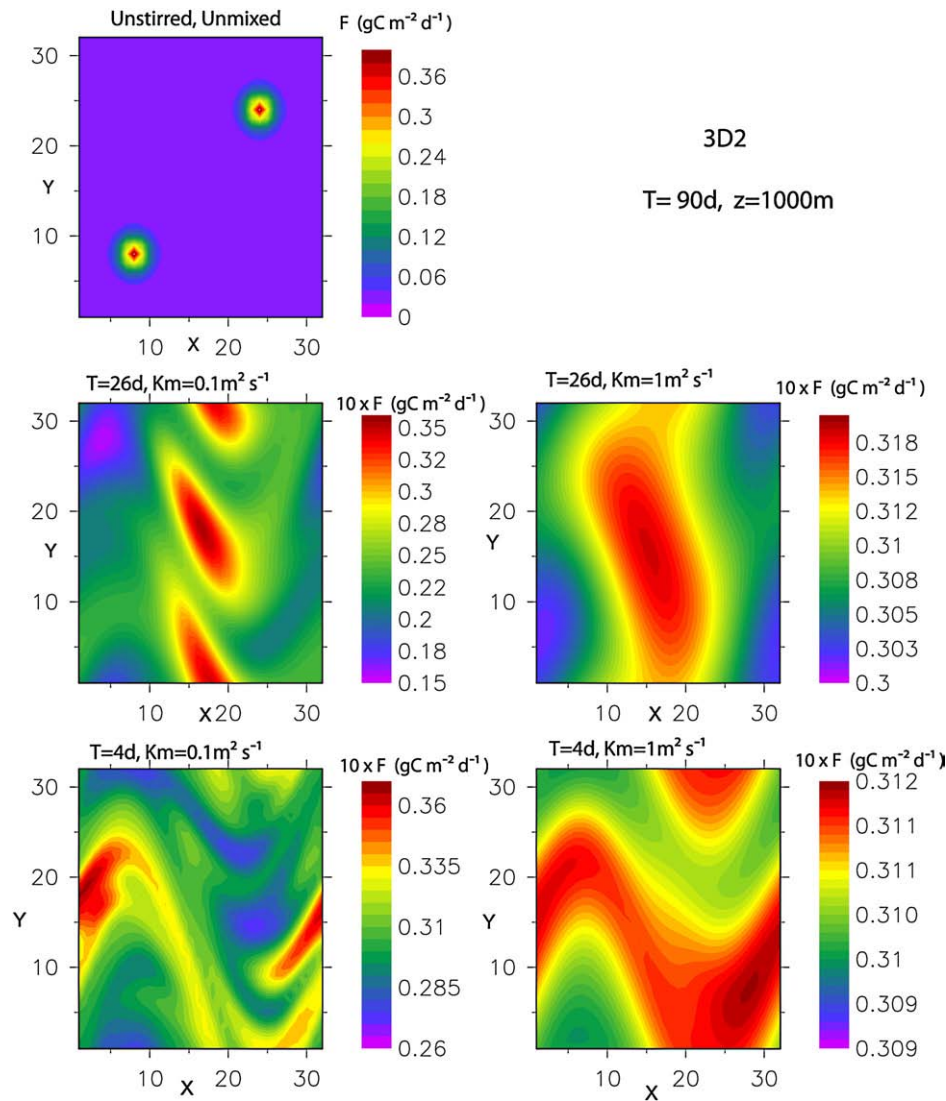


Fig. 6. Spatial distribution of  $F$  at  $t=90$  days and  $z=1000$  m Run 3D-2, for the unstirred case (upper left panel),  $T=26$  days (middle panels) and  $T=4$  days (lower panels), and with  $K_m=0.1 \text{ m}^2 \text{ s}^{-1}$  (left panels) and  $K_m=1 \text{ m}^2 \text{ s}^{-1}$  (right panels).

of increased stirring and mixing is to decrease the spatially averaged response of  $P$  while increasing that of  $Q$ .  $P_{\max}$  and  $Q_{\max}$  values evolve to  $(2.8; 10.9) \text{ mg C m}^{-3}$  for  $T=26$  days and  $(5.1; 17.4) \text{ mg C m}^{-3}$  for  $T=4$  days. The bloom in  $P$  is suppressed while that in  $Q$  is increased. In addition there is a greater reduction in  $F$ . Instead of the system tending to the well-mixed case (Run 1D-2: see Figs. 1 and 2), for the values of stirring and mixing considered, the system close to the TMZ is pushed into a high  $Q$ , low  $P$  regime. The reason is the flux at the TMZ is stationary in space. Water parcels just below the TMZ are advected through regions of alternately high and low flux. To converge to the well-mixed limit close to the TMZ we require a mixed down depth on the order of a few meters.

Despite the very different conditions near the TMZ we do see a convergence to the well-mixed case at depth. In particular the speed of propagation of the second pulse in  $F$  changes to that of the falling particles at around  $400 \text{ m}$  ( $300 \text{ m}$  from the TMZ) for  $T=4$  days resulting in the pulse in the export flux arriving at around Day 140 (Fig. 9), which is very similar to that for Run 1D-2 (Fig. 2b). With  $T=26$  days, and a greater mix-down depth, the second peak in export flux remains suppressed, as in the case with no stirring. With increased diffusion ( $K_m=1 \text{ m}^2 \text{ s}^{-1}$ ), and the associated decrease in mix-down depth (Table 4), the signal in export flux is very close to that for Run 1D-2 (not shown) for both  $T=4$  and 26 days, emphasizing the

importance of the mix-down depth in determining the behavior of the system.

Finally, we compare the spatial variability vs. the spatial mean of the annual mean export flux (at  $1000 \text{ m}$ , the BMZ). The spatial mean and spatial standard deviation of the export flux annually averaged are given in Table 5 for the unstirred and the four stirred and mixed cases considered, as a fraction of the spatially averaged flux at the TMZ,  $F_o (=0.1 \text{ g C m}^{-2} \text{ day}^{-1})$ . The spatial mean at the bottom varies by only 3%. The standard deviation, however, varies considerably. Without stirring the standard deviation is two times that of the mean, reflecting the spatial variation of the flux at the TMZ. Stirring and mixing dramatically reduces spatial variability in the flux. With  $T=26$  days,  $K_m=0.1 \text{ m}^2 \text{ s}^{-1}$ , the standard deviation is only 5% of the mean. Increasing the stirring rate decreases this value still further. With  $K_m=1 \text{ m}^2 \text{ s}^{-1}$  the standard deviation is negligible.

The probability density function (PDF) of the annual mean export flux at  $1000 \text{ m}$  (the BMZ) at each horizontal grid point, together with the PDF of the timing of the maximum flux, also at each horizontal grid point, is shown in Fig. 10 for the two stirred cases with  $K_m=0.1 \text{ m}^2 \text{ s}^{-1}$ . The PDF of the annual mean is relatively narrow in both cases. The maximum difference of the annual mean flux at a grid point from the spatial mean is 15% of the spatial mean for  $T=26$  days (Fig. 10a) and only 2% for  $T=4$  days (Fig. 10c). The PDFs of the timing,

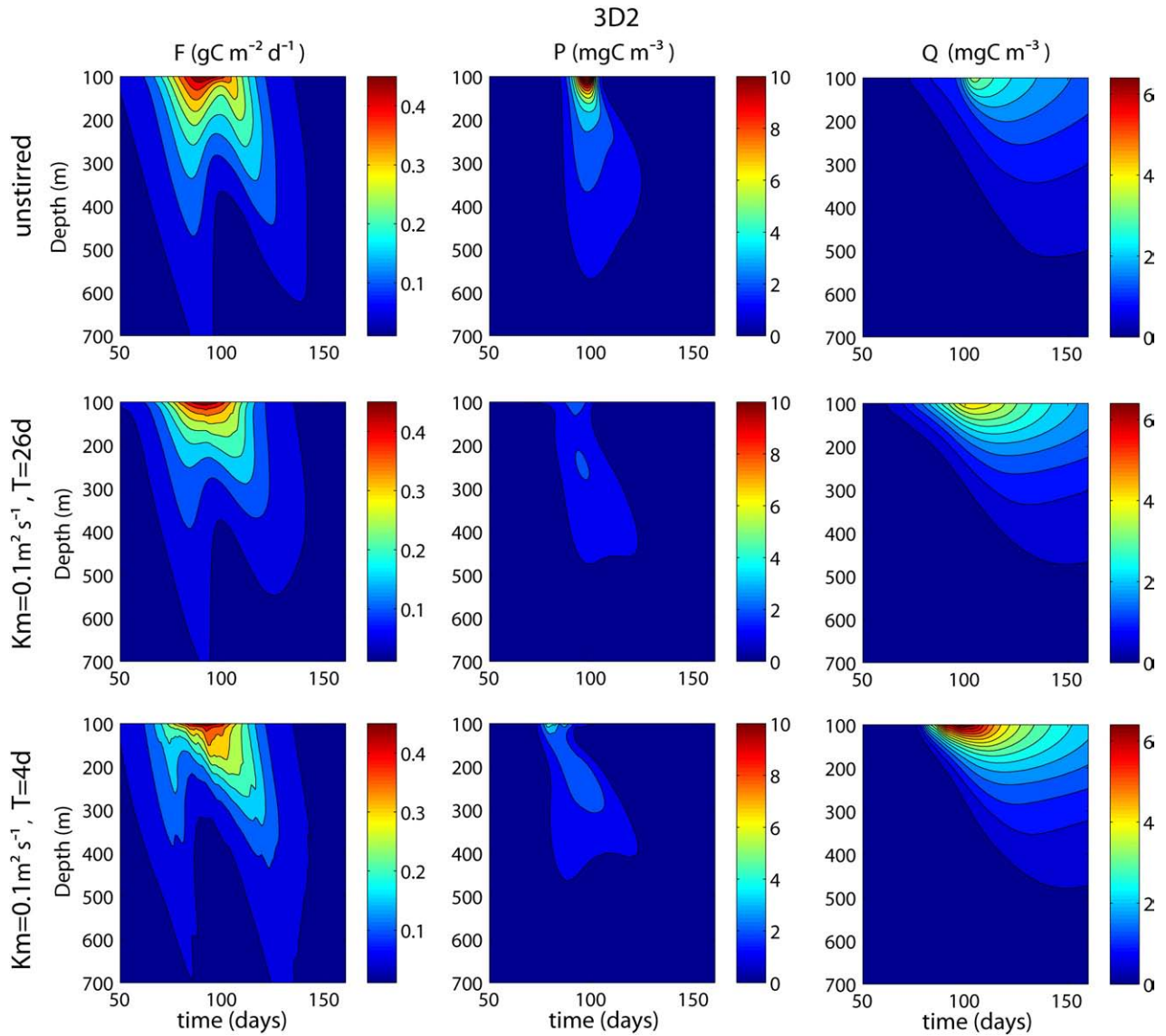


Fig. 7. Spatially averaged  $F$  (first column),  $P$  (second column),  $Q$  (third column) plotted against depth (m) and time (d) for Run 3D-2 for the: unstirred case (upper);  $T=26$  days  $K_m=0.1 \text{ m}^2 \text{ s}^{-1}$  (middle);  $T=4$  days and  $K_m=0.1 \text{ m}^2 \text{ s}^{-1}$  (lower).

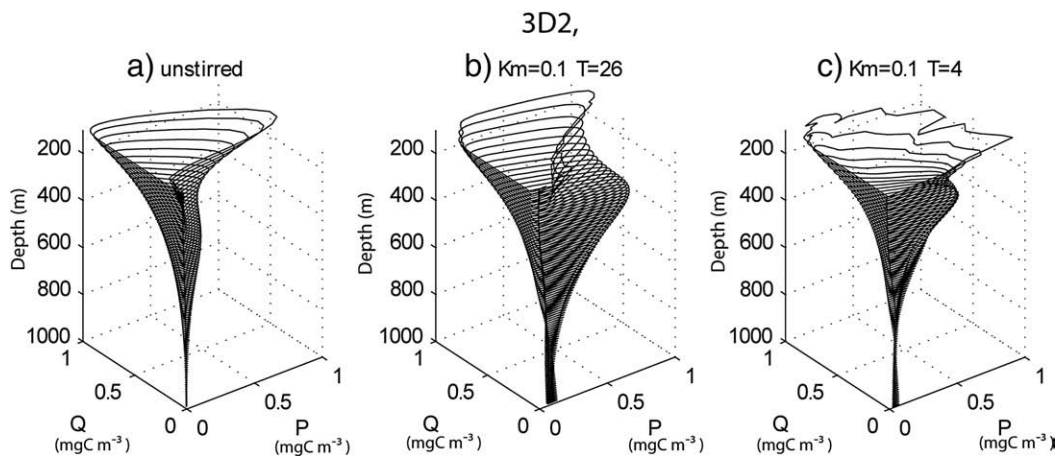
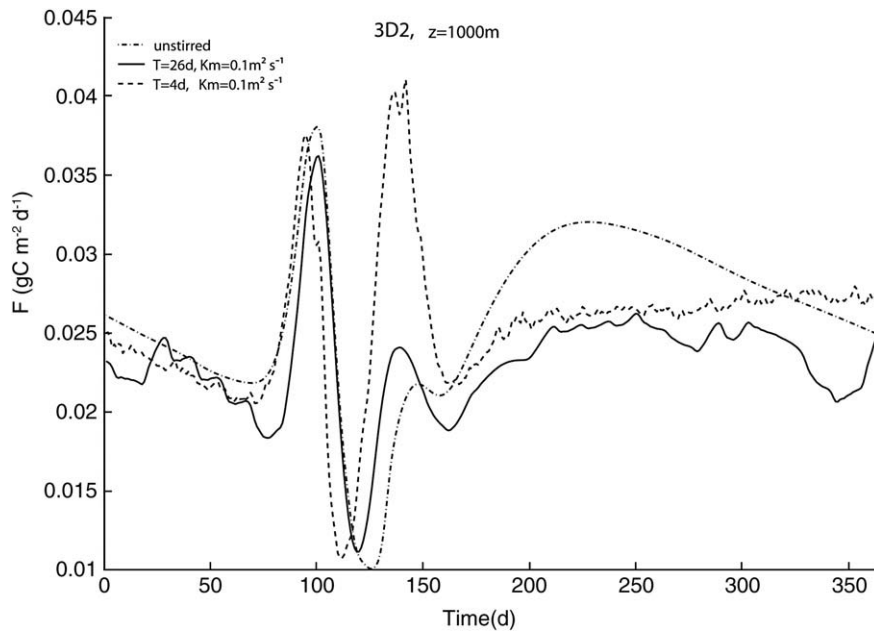


Fig. 8. Three-dimensional phase plots. Variation in the concentration of  $P$  and  $Q$  as a function of depth (in meters) for the 3 cases shown in Fig. 7.  $P$  and  $Q$  concentrations are normalized by their maximum values respectively.



**Fig. 9.** Spatially averaged exported flux at 1000 m for Run 3D-2 for the unstirred case (dashed-dotted line) for  $T=26$  days (solid lines) and  $T=4$  days (dash lines) and with  $K_m=0.1 \text{ m}^2 \text{ s}^{-1}$ .

however, are very different. With  $T=4$  days (rapid stirring) the PDF of the timing of the maximum flux at individual grid points is bimodal (Fig. 10d), reflecting the two peaks of similar magnitude found in the spatial mean (Fig. 9). Approximately 60% of the horizontal grid points have a maximum in their export flux around Day 140, which can be related to the second (and larger) peak in the spatial mean. With  $T=26$  days, the timing of the maximum exported flux at individual grid points is spread throughout the year (Fig. 10b). Only 4% of these timings occur within 10 days of the timing of the maximum of the spatial mean, which is approximately Day 100 (see Fig. 9). The majority (80%) occur after Day 200, suggesting that, in this particular case, it would be difficult to relate the timing of the export flux to the timing of the near TMZ bloom from a single point measurement.

#### 4. Summary and discussion

In order to elucidate the controls on fluxes and remineralization in the twilight zone, it is important to go beyond the use of empirical relationships that neglect physical and biological mechanisms (e.g. Martin et al., 1987; Armstrong et al., 2002). Here we present an extension of the two-dimensional (depth–time) flux–prey–predator model of Jackson and Burd (2002) to include the effects of spatial and temporal inhomogeneities, which are ubiquitous features of the marine environment. The goal has been to be illustrative rather than definitive and hence the prescribed spatial and temporal variability in the flux have relatively simple forms. The results, however, do highlight the fact that particle–biological interactions are very much affected by the way the surface flux is distributed in time and space as well as the subsequent lateral stirring and mixing by eddying motions as the particles sink.

Changing the temporal and spatial distributions of the surface produces only a modest change in the total export flux at the bottom

of the model layer. The largest change found here is brought about by packaging the flux into short bursts in time (Run 1D-2), but even then the change is only 25% of the export flux at that level compared to when the temporal distribution is less peaked (Run 1D-1).

There are much bigger changes in the timing and strength of pulses in the particle flux reaching the bottom of the layer. In all cases considered the initial increase in particle flux brought on by the start of the “bloom” is interrupted by a period of reduced flux caused by the rapid reaction of the near-surface particle feeders. The subsequent temporal behavior depends on the response of the near-surface carnivores ( $Q$ ) and the mid-water biology. A relatively rapid response of the near-surface  $Q$  suppresses  $P$  and allows a second pulse of high flux. The speed of the downward propagating signal of high flux is slowed by the response of the particle feeders. In the case of a spatially distributed surface flux, the large biological activity in regions of high flux is enough to delay and broaden, significantly, the pulse of the spatially averaged flux reaching the bottom.

As in the euphotic zone, the overwintering of the predator ( $Q$ ) in the system does affect the initial response of the prey ( $P$ ) to a new supply of food ( $F$ ) and thus the subsequent temporal evolution of the system. The choice of spatial variation of the surface flux used does introduce a spatial variation in the overwintering  $Q$ . Again this should be seen as illustrative of the effects of spatial variations in the overwintering predator. A different choice of spatial variation in  $F$  would produce a different relationship between  $F$  and  $Q$  and may well affect the impact of the spatial variability.

The inclusion of lateral stirring and mixing affects both the near-surface and deeper responses of the system but in different ways. The near-surface response for moderate stirring and mixing is to move the system to a high  $Q$ , low  $P$  regime. This response is caused by the somewhat artificial nature of the imposed spatially stationary surface flux, which in practice will move. The results are interesting

**Table 5**

Spatial mean and spatial standard deviation of the annual mean export flux for the unstirred case and the four stirred and mixed cases considered.

Annual flux ( $z=1000 \text{ m}$ )	Unstirred, unmixed	$T=26 \text{ days}$ $K_m=0.1 \text{ m}^2 \text{ s}^{-1}$	$T=4 \text{ days}$ $K_m=0.1 \text{ m}^2 \text{ s}^{-1}$	$T=26 \text{ days}$ $K_m=1 \text{ m}^2 \text{ s}^{-1}$	$T=4 \text{ days}$ $K_m=1 \text{ m}^2 \text{ s}^{-1}$
Spatial mean	$0.26 F_0$	$0.23 F_0$	$0.25 F_0$	$0.25 F_0$	$0.25 F_0$
Standard deviation	$0.5 F_0$	$1.14 \times 10^{-2} F_0$	$1.33 \times 10^{-3} F_0$	$5.15 \times 10^{-4} F_0$	$2.81 \times 10^{-5} F_0$

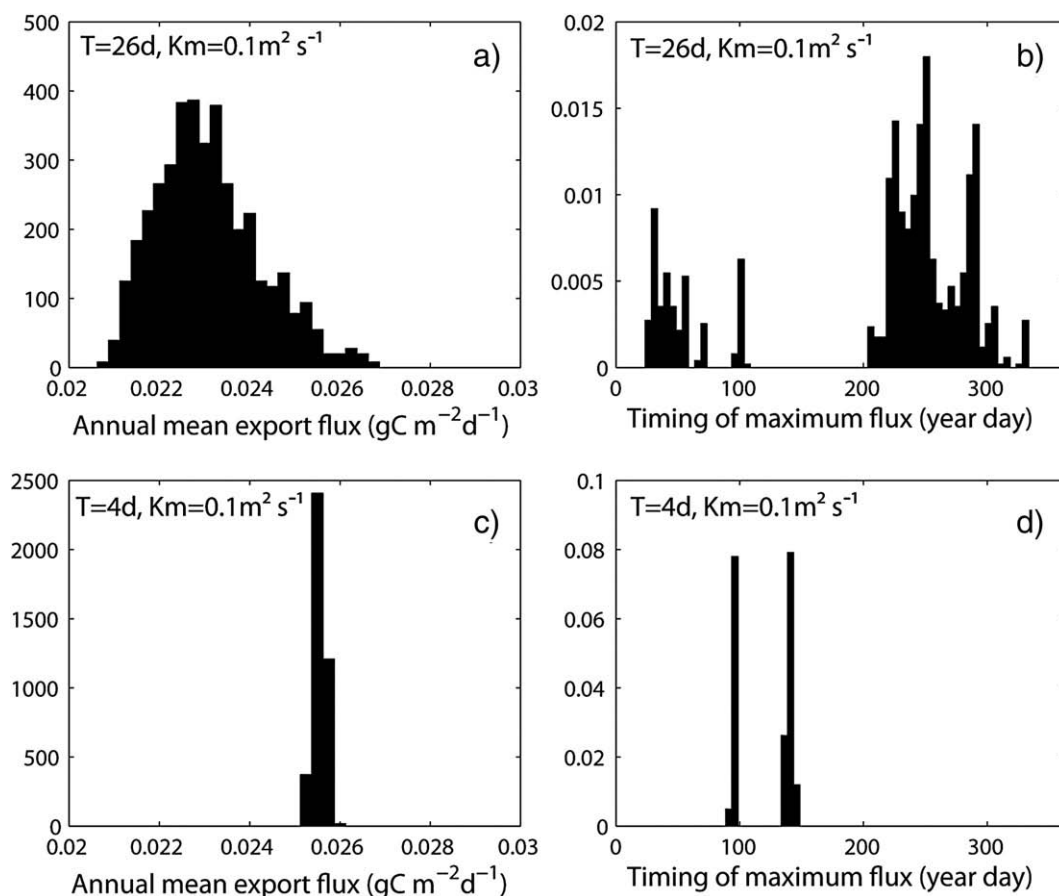


**Fig. 10.** Probability density functions (PDFs) for the annual mean export flux and timing of the maximum flux at individual grid points for the two stirred cases with  $K_m = 0.1 \text{ m}^2 \text{ s}^{-1}$ :  $T = 26$  days (a and b),  $T = 4$  days (c and d).

nonetheless in showing a non-monotonic trend in the system response in going from the unstirred to the well-mixed state. Surprisingly, and perhaps fortunately, the near-surface response does not unduly affect the mid-water response where we find as expected that increased stirring and mixing pushes the system to the well-mixed limit. A useful metric in determining the impact of stirring and mixing is the mix-down depth discussed in Section 3.2 which combines the effects of the initial patch size, strength of stirring, diffusion and sinking rate. When the mix-down depth is small compared to the depth to which biological interactions are important, then the impact of stirring and mixing is large, producing significant changes to the temporal behavior of the export flux and reducing spatial inhomogeneities.

The behavior of the biological system is strongly controlled by a number of parameters that are poorly constrained by literature values. We have set these parameters to values suggested by Jackson and Burd (2002) (who investigated the sensitivity of the particle-biological system to a number of these parameters). Caution needs to be exercised if applying our results to model systems that have very different parameter values (or ecosystem dynamics), although the qualitative nature of the results may well hold. One aspect that deserves discussion is the sinking rate. The sinking rate chosen in this study,  $30 \text{ m day}^{-1}$ , is in the accepted limits for marine aggregates (for a size  $> 0.15 \text{ mm}$ ) found in a number of studies (Fowler et al., 1987; Alldredge and Gotschalk, 1988; Alldredge and Silver, 1988; Diercks and Asper, 1997; Stemmann et al., 2002; Hood et al., 2003). More recent estimates suggest that the global average sinking rate may be in excess of  $100 \text{ m day}^{-1}$  (c.f. Guidi et al., 2008). Increasing the sinking rate,  $v$ , increases both the biological depth scale,  $L_b$ , (given approximately by  $1/k$ ; Eq. (3)) and the mix-down depth,  $L_d$  (Eq. (7)). We therefore expect an increase in the spatially averaged export flux

with greater spatial inhomogeneity, the latter of which has implications for sampling the flux (see below).

Considering the physical model, we have used a simple horizontal velocity field which is uniform with depth and in addition ignored vertical motions. In reality the situation is more complex with the source of particles often related to the flow itself. The flow topology affects the stirring and mixing characteristics as well as the location of regions of strong primary production (see e.g. Martin, 2003; Lehahn et al., 2007), an aspect that should be included in future studies.

*Sampling considerations:* As demonstrated in this study, spatial and temporal heterogeneities in the flux at the bottom of the euphotic zone, combined with stirring and mixing in the water column, can strongly modulate the degradation rate of the flux and the eventual export from the mesopelagic zone. Relating the export flux to surface primary production rates (as attempted by Lampitt and Antia, 1997, for example) therefore is problematic. Even in the spatially homogenous case the arrival time of pulses of the flux of carbon is affected by mid-water biology producing an apparent sinking rate that may be very different from that of the particles themselves. Compare, for instance, the early arrival of the flux in 1D-2 with high bacterial degradation rate (implying an apparent sinking rate of  $50 \text{ m day}^{-1}$ ) with the late arrival in 1D-1 (apparent sinking rate  $3 \text{ m day}^{-1}$ ), while the imposed particle sinking rate in the experiments is  $30 \text{ m day}^{-1}$ . Spatial inhomogeneities in the surface flux produce inhomogeneities in the export flux, the level depending on the amount of lateral stirring and mixing.

Because traditional sampling techniques (traps, *in situ* pumps) in the mesopelagic layer are not adapted for resolving the mesoscale (Gorsky et al., 2002), the mesoscale distribution of aggregates or fluxes has been seldom reported. The depth distribution of inhomogeneities remains unknown limiting our ability to assess the representativeness of point measurements.

Buesseler et al. (2007) report on observations using drifting sediment traps to measure the transfer efficiency of sinking particulate organic carbon. Using the semi-Lagrangian technique they are able to connect the fluxes at different depths and obtain consistent transfer efficiencies. In terms of gaining a spatial average of fluxes, however, the technique is limited. In regions where properties are poorly mixed at a particular depth the spatial variations of the flux can be large (c.f. Fig. 7). Fixed (Eulerian) measurements can be at an advantage. An eddying flow sweeps the variability in particle flux past the sampling point, considerably reducing the variable in the estimated annual mean (Table 5 and Fig. 10). There may, however, still be problems in determining the timing of the maximum in the flux (Fig. 10). A judicious combination of Lagrangian and Eulerian sampling will provide estimates of rates of processes and areal means. Determining the benefits of different sampling strategies is beyond the scope of the present paper, but a model similar to the one presented here, perhaps with improved physics and biogeochemistry, could provide a tool in the planning of observations and the interpretation of results.

Clearly more complex flows, and their impact on the spatial and temporal characteristics of the generation of the particle flux, need to be considered in later studies. The aim of the present work, however, is to identify and expose some basic processes that impact on particle fluxes in the mesopelagic zone. The results should aid the interpretation of simulations which incorporate more complex biological and flow regimes. The importance of correctly modeling physical processes in marine ecosystem modeling studies cannot be overstated. The time and space scales of the physics in which an ecosystem model is embedded have to be consistent with the ecosystem itself (Hood et al., 2003; Friedrichs et al., 2006).

## Acknowledgments

This work has been funded by NSF grant OCE 0424860. We wish to thank Adrian Martin for the sharing of the numerical code for the lateral advection of tracers (IPRC/SOEST publication number 688/7922).

## References

- Allredge, A.L., Gotschalk, C., 1988. In situ settling behavior of marine snow. *Limnology and Oceanography* 33 (3), 339–351.
- Allredge, A.L., Silver, M.W., 1988. Characteristics, dynamics and significance of marine snow. *Progress in Oceanography* 20, 41–82.
- Andersson, J.H., Wijsman, J.W., Herman, P.M.J., Middelburg, J.J., Soetaert, K., Heip, C., 2004. Respiration patterns in the deep ocean. *Geophysical Research Letters* 31, L03304. doi:10.1029/2003GL018756.
- Armstrong, R.A., Lee, C., Hedges, J.I., Honjo, S., Wakeham, S.G., 2002. A new, mechanistic model for organic carbon fluxes in the ocean based on the quantitative association of POC with ballast minerals. *Deep-Sea Research II* 49, 219–236.
- Baker, D.F., 2007. Reassessing carbon sinks. *Science* 317, 1708–1709.
- Buesseler, K.O., Lamborg, C.H., Boyd, P.W., Lam, P.J., Trull, T.W., Bidigare, R.R., et al., 2007. Revisiting carbon flux through the ocean's twilight zone. *Science* 316 (5824), 567–570 New York, N.Y.
- Dadou, I., Garçon, V., Andersen, V., Flier, G.R., Davis, C.S., 1996. Impact of the North Equatorial Current meandering on a pelagic ecosystem: a modeling approach. *Journal of Marine Research* 54, 311–342.
- Diercks, A.R., Asper, V.L., 1997. In situ settling speeds of marine snow aggregates below the mixed layer: Black sea and Gulf of Mexico. *Deep-Sea Research* 44 (3), 386–398.
- Doney, S.C., Kleypas, J.A., Sarmiento, J.L., Falkowski, P.G., 2002. The US JGOFD synthesis and modeling project — an introduction. *Deep-Sea Research II* 49, 1–20.
- Fowler, S.W., Buat-Menard, P., Yokoyama, Y., Ballestra, S., Holm, E., Van Nguyen, H., 1987. Rapide removal of Chernobyl fallout from Mediterranean surface waters by biological activity. *Nature* 329, 56–58.
- Friedrichs, M.A.M., Hood, R.R., Wiggert, J.D., 2006. Ecosystem model complexity versus physical forcing: quantification of their relative impact with assimilated Arabian Sea data. *Deep-Sea Research II* 53 (5–7), 576–600.
- Garrett, C., 1983. On the initial streakiness of a dispersing tracer in two- and three-dimensional turbulence. *Dynamics of Atmospheres and Oceans* 7 (4), 265–277.
- Gorsky, G., Prieur, L., Taupier-Letage, I., Stemann, L., Picheral, M., 2002. Large particulate matter in the western Mediterranean I, LPM distribution related to mesoscale hydrodynamics. *Journal of Marine System* 33, 289–311.
- Guidi, L., Jackson, G.A., Stemann, L., Miquel, J.C., Picheral, M., Gorsky, G., 2008. Relationship between particle size distribution and flux in the mesopelagic zone. *Deep-Sea Research* 55 (10), 1364–1374.
- Hood, R.R., Kohler, K.E., McCreary, J.P., Smith, S.L., 2003. A four-dimensional validation of a coupled physical–biological model of the Arabian Sea. *Deep-Sea Research II* 50 (22–26), 2917–2945.
- Hu, Y., Pierrehumbert, R.T., 2001a. The advection–diffusion problem for stratospheric flow: part II. Probability distribution function of tracer gradients. *Journal of Atmospheric Sciences* 59, 2830–2845.
- Hu, Y., Pierrehumbert, R.T., 2001b. The advection–diffusion problem for stratospheric flow: part I. Concentration probability distribution function. *Journal of Atmospheric Sciences* 58, 1493–1510.
- Jackson, G.A., Burd, A.B., 2002. A model for the distribution of particle flux in the mid-water column controlled by subsurface biotic interactions. *Deep-Sea Research II* 49 (1–3), 193–217.
- Jahnke, R.A., 1996. The global ocean flux of particulate organic carbon: areal distribution and magnitude. *Global Biogeochemical Cycles* 10, 71–88.
- Lampitt, R.S., Antia, A.N., 1997. Particle flux in deep seas: regional characteristics and temporal variability. *Deep-Sea Research* 44 (8), 1377–1403.
- Laws, E., 2004. Export flux and stability as regulators of community in pelagic marine biological communities: implications for regime shifts. *Progress in Oceanography* 60, 343–354.
- Ledwell, J.R., Watson, A.J., Law, C.S., 1998. Mixing of a tracer in the pycnocline. *Journal of Geophysical Research* 103 (C10), 21,499–21,529.
- Lehahn, Y., d'Ovidio, F., Lévy, M., Heifetz, E., 2007. Stirring of the northeast Atlantic spring bloom: a Lagrangian analysis based on multisatellite data. *Journal of Geophysical Research* 112. doi:10.1029/2006JC003927.
- Martin, A.P., 2003. Phytoplankton patchiness: the role of lateral stirring and mixing. *Progress in Oceanography* 57, 125–174.
- Martin, J.H., Knauer, G.A., Karl, D.M., Broenkow, W.W., 1987. VERTEX: carbon cycling in the Northeast Pacific. *Deep-Sea Research* 34 (2), 267–285.
- Neufeld, Z., Lopez, C., Hernandez-Garcia, E., Piro, O., 2002. Excitable media in open and closed chaotic flows. *Physical Review E* 66, 066208. DOI: 10.1103.
- Pierrehumbert, R.T., 1994. Tracer microstructure in the large-eddy dominated regime. *Chaos, Solitons and Fractals* 4, 1091–1110.
- Richards, K.J., Brentnall, S.J., 2006. The impact of diffusion and stirring on the dynamics of interacting populations. *Journal of Theoretical Biology* 238, 340–347.
- Smith, K.L.J., Kaufmann, R.S., 1999. Long-term discrepancy between food supply and demand in the deep eastern North Pacific. *Science* 284, 1174–1177.
- Smolarkiewicz, P.K., 1983. A simple positive definite advection scheme with small implicit diffusion. *Monthly Weather Review* 479–486.
- Smolarkiewicz, P.K., Clark, T.L., 1986. The multidimensional positive definite advection transport algorithm: further development and applications. *Journal of Computational Physics* 67, 396–438.
- Smolarkiewicz, P.K., Grabowski, W.W., 1990. The multidimensional positive definite advection transport algorithm: nonoscillatory option. *Journal of Computational Physics* 86, 355–375.
- Smolarkiewicz, P.K., Margolin, L.G., 1998. MPDATA: a finite-difference solver for geophysical flows. *Journal of Computational Physics* 140, 459–480.
- Stemann, L., Gorsky, G., Marty, J.C., Picheral, M., Miquel, J.C., 2002. Four-year study of large-particle vertical distribution (0–1000 m) in the NW Mediterranean in relation to hydrology, phytoplankton, and vertical flux. *Deep-Sea Research II* 49 (11), 2143–2162.
- Stemann, L., Jackson, G.A., Ianson, D., 2004a. A vertical model of particle size distributions and fluxes in the midwater column that includes biological and physical processes — part I: model formulation. *Deep-Sea Research* 51 (7), 865–884.
- Stemann, L., Jackson, G.A., Gorsky, G., 2004b. A vertical model of particle size distributions and fluxes in the midwater column that includes biological and physical processes — part II: application to a three year survey in the NW Mediterranean Sea. *Deep-Sea Research* 51 (7), 885–908.
- Stemann, L., Prieur, L., Legendre, L., Taupier-Letage, I., Picheral, M., Guidi, L., Gorsky, G., 2008. Effects of frontal processes on marine aggregate dynamics and fluxes: an interannual study in a permanent geostrophic front (NW Mediterranean). *Journal of Marine Systems* 70, 1–20.
- Thuburn, J., Tan, D.G.H., 1997. A parameterization of mixdown time for atmospheric chemicals. *Journal of Geophysical Research* 102, 13037–13049.
- Tortell, P.D., Payne, C.D., Li, Y., Trimborn, S., Rost, B., Smith, W.O., Riesselman, C., Dunbar, R.B., Sewick, P., 2008. CO<sub>2</sub> sensitivity of Southern Ocean phytoplankton. *Geophysical Research Letters* 35, L04605. doi:10.1029/2007GL032583.
- Young, W.R., Rhines, P.B., Garrett, C.J.R., 1982. Shear-flow dispersion, internal waves and horizontal mixing in the ocean. *Journal of Physical Oceanography* 12, 515–527.